ACS Photonics

Article

pubs.acs.org/journal/apchd5

Core/Alloyed-Shell Quantum Dot Robust Solid Films with High Optical Gains

Chun Hao Lin,[†] Evan Lafalce,[‡] Jaehan Jung,[†] Marcus J. Smith,[†,§] Sidney T. Malak,[†] Sandip Aryal,[‡] Young Jun Yoon,[†] Yaxin Zhai,[‡] Zhiqun Lin,[†] Z. Valy Vardeny,[‡] and Vladimir V. Tsukruk*[,†]

[†]School of Materials Science and Engineering, Georgia Institute of Technology, Atlanta, Georgia 30332, United States

[‡]Department of Physics and Astronomy, University of Utah, Salt Lake City, Utah 84112, United States

[§]Aerospace Systems Directorate, Air Force Research Laboratory, Wright-Patterson Air Force Base, Fairborn, Ohio 45433, United States

Supporting Information

ABSTRACT: We report high optical gain from freestanding, optically stable, and mechanically robust films that are loaded with cross-linked CdSe/$Cd_{1-x}Zn_xSe_{1-y}S_y$ core/alloyed shell quantum dots (QD). These solid films display very high net optical gain as high as 650 cm^{-1} combined with a low pump excitation gain threshold of 44 $\mu J/cm^2$. The functionalization of the QDs using short-chain bifunctional cross-linkers not only significantly improves the net optical gain by allowing for a nearly 2-fold increase in QD loading but also provides stable passivation of the QDs which imparts excellent thermal stability, mechanical robustness, and stability under harsh chemical environments. The gain achieved here is up to 3-fold higher than that typically reported for traditional drop-cast QD films. Moreover, stable photoluminescence over long shelf storage time is a distinguished characteristic of the films. The QD films fabricated here span large areas (several cm^2), can be readily micropatterned and sustain multiple harsh chemical treatment. Furthermore, they can be readily transferred onto different substrates without compromising their structural integrity and without diminishing optical activity that opens the paths to design complex and robust gain−loss optical structures.

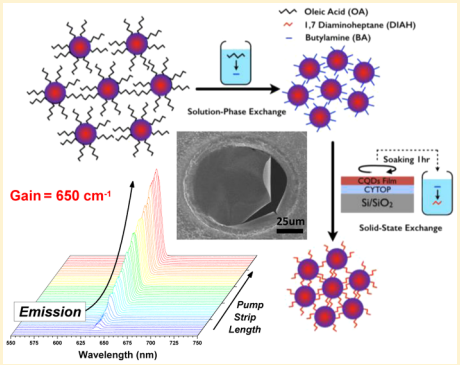

KEYWORDS: *optical gains, amplified spontaneous emission, bifunctional cross-linkers, cross-linked quantum dots film*

The ability to develop stable, high-performance optical gain media with tunable emission from the visible to infrared spectral regions promises new opportunities in flexible lasing devices. Highly emissive colloidal nanocrystals are emerging materials for semiconductor laser action since they exhibit size-dependent optoelectronic properties due to exciton quantum confinement.[1−5] A rich variety of colloidal nanocrystals have been recently synthesized as potential candidates for optical gain media, including Cd- and Pb-based quantum dots (QDs),[6−9] CdSe nanoplatelets,[10−13] and $CsPbX_3$ (X = Cl, Br, I) perovskite QDs.[14] Among them, CdSe nanoplatelets have shown one of the highest net gain value of 500−690 cm^{-1} in the green and red spectral range due to their large oscillator strength in comparison to that of QDs, whereas $CsPbBr_3$ perovskite QD films possess a net gain value of 450 cm^{-1} in the green spectral range. The high net gain value exhibited by these materials is widely recognized as an important "figure of merit" to consider when developing new photonic systems that demonstrate parity-time symmetry, which requires a sensitive balance between optical gain and loss to achieve the breaking point for single-mode lasing,[15,16] double refraction systems,[17] and directional invisibility and reflection.[18,19]

Although net gain values are high in the above-mentioned materials, the colloidal and photoluminescence (PL) stabilities remain as important obstacles that need to be addressed before realizing practical photonic structures. In this regard, the PL intensity in the vast majority of studies to date is not stable and long lasting even under modest external effects such as light illumination, chemical treatment, or mechanical rubbing. These persistent issues are caused by the poor physical stability of poorly controlled simple drop-cast films as well as photo-oxidation processes in/on quantum dots.

For example, the lasing output intensity of CdSe nanoplatelets is reduced to 10%−50% of the original value within 1 h under continuous-wave pumping.[10] Furthermore, the surface of these CdSe structures is highly sensitive to polar solvents, which can lead to an irreversible physical stacking and thus a large reduction of PL intensity due to the efficient energy transfer to defective nanoplatelets.[20] As for the PL stability in $CsPbX_3$ perovskite QDs, it is reported that the PL of $CsPbI_3$ perovskite QDs in the red spectral range gradually vanishes because these materials undergo a structural phase transition

Received: December 23, 2015
Published: March 2, 2016

DOI: 10.1021/acsphotonics.5b00743
ACS Photonics 2016, 3, 647−658

from the PL-active cubic to the PL-inactive orthorhombic structure.[14] A recent study also shows a fast (within minutes) photodegradation of $CsPbBr_3$, $CsPbBr_xI_{3-x}$, and $CsPbI_3$ perovskite QDs, exemplifying their highly unstable PL emission.[21]

In stark contrast to these unstable materials, the well-developed Cd-based QDs possess relatively high colloidal stability and stable emission in the visible region,[22] making them promising candidates for the fabrication of stable photonic devices if incorporated in polymer films and coatings.[23] However, the typical net gain value of Cd-based QDs in solid state (mostly, drop-cast films) is relatively low (60−200 cm^{-1}), which is well below those reported in CdSe nanoplatelets and $CsPbBr_3$.[8,24,25] Moreover, the film integrity of QDs capped with monodentate ligands can easily deteriorate during common fabrication processes due to the good solubility of the organic capping ligands in a variety of nonpolar solvents.

Most studies in the area of Cd-based QDs have focused on the sophisticated engineering of the core/shell structure in order to suppress the Auger recombination rate (AR).[7,8] To date, little attention has been paid to how modification of the ligand can affect gain performance and PL stability of the QD films.[26,27] This is in striking contrast to other fields where ligand engineering has attracted great attention since it can significantly improve device performance.[28−31] Interestingly, a recent study has reported a very high gain in Cd-based QD films that were capped with the inorganic halide due to the maximized packing density.[32] Moreover, some studies have shown that ligand engineering can be utilized to impart mechanical strength using bifunctional cross-linkers to form cross-linked and mechanically robust QD solids.[33,34] These studies suggest that the ligand replacement can be an effective way to improve both the performance and the mechanical strength of the QD materials and suppress material degradation caused by a loss of passivation on the QD surface.

In the present work, we report the crafting of freestanding, mechanically robust, and optically, environmentally, and chemically stable $CdSe/Cd_{1-x}Zn_xSe_{1-y}S_y$ core/alloyed-shell QD films with outstanding net gain values up to 650 cm^{-1}, minimum optical losses around 50 cm^{-1}, and amplified spontaneous emission (ASE) thresholds as low as 44 $\mu J/cm^2$ in the quasi-continuous wave (q-CW) region (ns pulse excitation). These results are achieved by capitalizing on the rationally designed cross-linkable core/alloyed-shell QDs with short bifunctional ligands. Two consecutive strategies were implemented to achieve stable high gain properties in the resulting film with highly loaded cross-linked QDs. The first strategy involves the maximization of QD-loading density by replacing the long ligand oleic acid (OA) with the shorter ligand butylamine (BA). This ligand replacement greatly increases the QD packing density up to ∼50%, which is nearly 2-fold higher than that of conventional QD films reported to date and is in fact closer to the theoretical limit (52% for simple cubic to 74% for face centered cubic for sphere packing without capping ligands).

The second complementary strategy is to further impart mechanical strength, chemical resistance, and optical stability by exposure to a bifunctional cross-linker 1,7 diaminoheptane (DIAH). The bifunctional cross-linker rendered a very stable passivation of the QD surface by connecting (i.e., cross-linking) the adjacent QDs via the strong coordination interaction between $CdSe/Cd_{1-x}Zn_xSe_{1-y}S_y$ core/alloyed shell QDs and the two terminal NH_2 groups of the DIAH linkers. The resulting cross-linked QD materials can be fabricated as mechanically robust large area films of several cm^2 across. Moreover, they can be readily released as a freestanding film and transferred onto different substrates without compromising their structural integrity and while retaining their stable optical activity under mechanical stresses and the harsh chemical environments under which traditional drop-cast films show a fast deterioration. Finally, we demonstrate that our designs are compatible with lithographical patterning techniques for the development of optical lasing arrays.

RESULTS AND DISCUSSION

The surface of as-synthesized QDs is protected with an organic shell of oleic acid (OA) (Figure 1; see Materials and Methods).

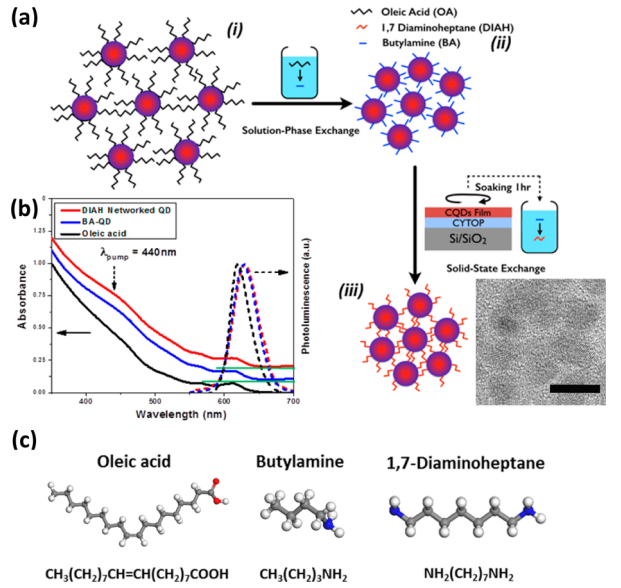

Figure 1. (a) Cross-linked QD solid film fabrication: the as-synthesized oleic acid (OA)-capped $CdSe/Cd_{1-x}Zn_xSe_{1-y}S_y$ core/alloyed-shell QDs (i) undergo the solution-phase ligand exchange by adding butylamine (BA) in the QD solution (ii); after the solution-phase ligand exchange, the concentrated BA-capped QD solution is cast to form a close-packed QD film, which is subsequently soaked in a 0.1 M methanol solution of 1,7 diaminoheptane (DIAH) to perform the solid-state ligand exchange. The cross-linked QDs are tethered with DIAH ligand and show tight packing (HRTEM scale bar is 10 nm) (iii). (b) Absorbance (solid) and emission (dashed) spectra of as-synthesized OA-capped QD solution (black line), BA-capped QD film (blue line), and DIAH-tethered QD film (red line). The baselines (green solid lines) of the BA-capped QD film and DIAH-tethered QD film are offset for clarity. (c) Molecular models and chemical formulas of the organic ligands used in this study: oleic acid (OA), butylamine (BA), and 1,7 diaminoheptane (DIAH).

The replacement of the OA ligand with shorter ligands was explored here to increase QD-loading and stabilize QD films. Because thiol functional groups tend to quench the PL intensity,[35] we chose amine-terminated ligands as candidates for stabilization and cross-linking of QDs.[36] Finally, excessively volatile ligands with a low melting point (m_p) and boiling point (b_p) can lead to fast thermal and physical deterioration, which can cause optical quenching due to the loss of surface passivation. Cross-linkers with higher m_p and b_p, as well as a lower vapor pressure, are expected to provide a surface passivation that is resistant to harsh environments and prevents the solid films from fast degradation during fabrication, usage, and storage. Thus, the shorter length of DIAH ligands (7 C−C

DOI: 10.1021/acsphotonics.5b00743
ACS Photonics 2016, 3, 647−658

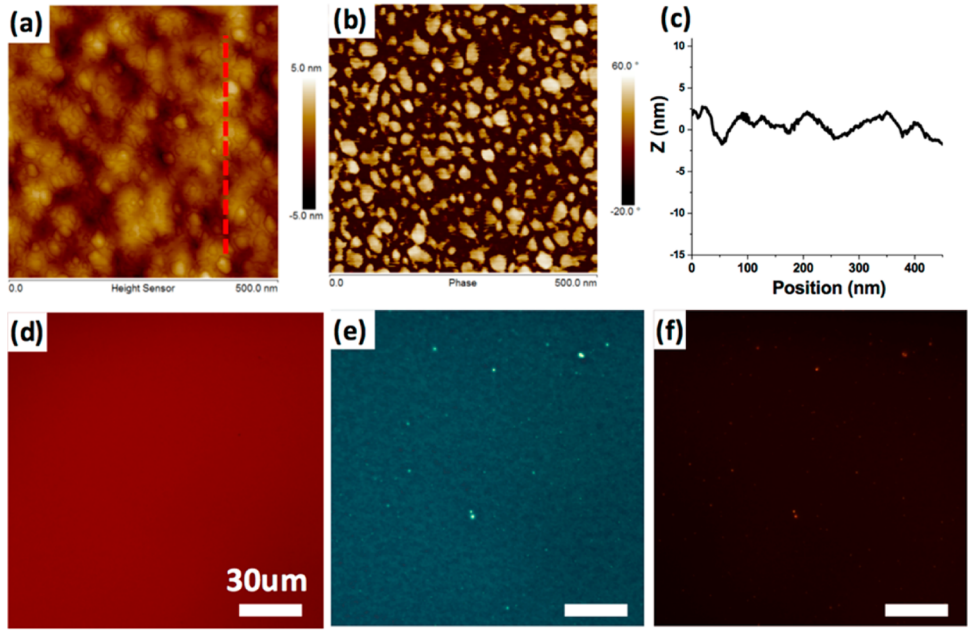

Figure 2. AFM scans of height (a), phase (b), and (c) height cross-section along the line in panel a for the DIAH-tethered QD film. The height scale is 10 nm, and the phase scale is 80°. Fluorescence imaging shows uniform emission over large areas (d), while bright field (e) and dark field (f) optical micrographs show uniform morphology with minimal physical defects. All scale bars are 30 μm.

bonds) and the much higher m_p of 26−29 °C and b_p of 223−225 °C should provide stable surface passivation under the elevated temperatures present during optical pumping (Table S1).[37]

Figure 1a illustrates the material processing steps utilized in this study. First, we synthesized chemical compositional gradient CdSe/$Cd_{1-x}Zn_xSe_{1-y}S_y$ core/alloyed-shell QDs with an average diameter of 8.2 nm by following a published procedure with some modifications.[38] These QD structures have been selected because of their high stability and enhanced quantum yield. In fact, the core/alloyed-shell or alloyed-core/shell QD structure has been reported to effectively increase the Auger recombination lifetime to at least a few hundred ps and even enable single exciton gain.[8,11,54] We then performed the subsequent solution-phase and solid-state ligand exchanges to tether CdSe/$Cd_{1-x}Zn_xSe_{1-y}S_y$ QDs with the DIAH ligand.

High resolution transmission electron microscopy (HR-TEM) confirmed the QD dimensions and allowed for the estimation of interparticle distance of QDs capped with different ligands (Figures 1 and S2) (see Materials and Methods). After the solution-phase ligand exchange from OA to BA, the distance between neighboring QDs decreases significantly from 3.2 ± 0.5 nm for OA-capped QDs to 1.1 ± 0.5 nm for BA-capped QDs. The reduced interparticle distance demonstrates the effective increase in QD loading after exchange with the shorter organic ligand shell. Furthermore, the spacing of the cross-linked films (i.e., DIAH-tethered QDs; 1.2 ± 0.4 nm) is similar to that of the BA-capped QD films, confirming that the loading is primarily controlled by the molecular dimensions of organic ligands.[27,39]

The optical properties of QDs (absorption and emission) in solution and solid film state are shown in Figure 1b. All samples have similar first excitonic absorption peaks near 610 nm, whereas the emission peak shows a red-shift of 9 nm in the condensed solid state (629 nm in solid film vs 620 nm in solution). Such a red-shift indicates higher optical reabsorption and modest coupling interactions between neighboring QDs that can induce enhanced interparticle energy transfer.[40,41] The cross-linking within solid films did not lead to further red-shifting, signifying the absence of excessive QD aggregation.

The spin-cast films from BA-capped QDs are uniform, without QD aggregation, and exhibit uniform PL emission. Atomic force microscopy (AFM) revealed that the film possesses a microroughness of 0.6 and 3.9 nm over surface areas of 500 nm by 500 nm and 10 μm by 10 μm (respectively), confirming a uniform material distribution (Figure S3a,b,i,j). The cross-linked DIAH-tethered QD films remain smooth with a microroughness of around 1 nm over surface areas of 500 nm by 500 nm and also exhibit a larger phase contrast which confirms the presence of the limited QD clusters surrounded by an organic matrix (Figures 2 and S3g,h).

Differential scanning calorimetry for the DIAH-tethered QD films shows a glass transition near 97 °C and no indication of a melting point, which is a characteristic of cross-linked and amorphous polymer films with restricted molecular mobility (Figure 5d).[42] Furthermore, comparative FTIR spectra for all films indicate a clear difference between BA-capped QD and DIAH-tethered QD films in the spectral range of C−H and N−H stretching mode bands. The large reduction of symmetric and asymmetric CH_3 stretching peaks and the absence of asymmetric N−H stretching peak indicate the cross-linking/coordination of ligands with the QD surface (see Materials and Methods and Figure S4).[43,44]

The optical performance of the DIAH-passivated QD solid films was studied using a standard configuration of the variable stripe length (VSL) method with q-CW nanosecond (ns) pulsed 440 nm laser excitation (see Materials and Methods).[45] As we observed, amplified spontaneous emission (ASE) from the close-packed QDs films can be clearly detected under q-CW conditions, which is rarely reported due to efficient Auger recombination rates that typically suppress ASE.[6] In fact, nearly all reported QD net gain values in the literature were measured using ultrafast femtosecond lasers to overcome the Auger recombination rate.[24,47,49] Although the 5 ns pulse duration is

DOI: 10.1021/acsphotonics.5b00743
ACS Photonics 2016, 3, 647−658

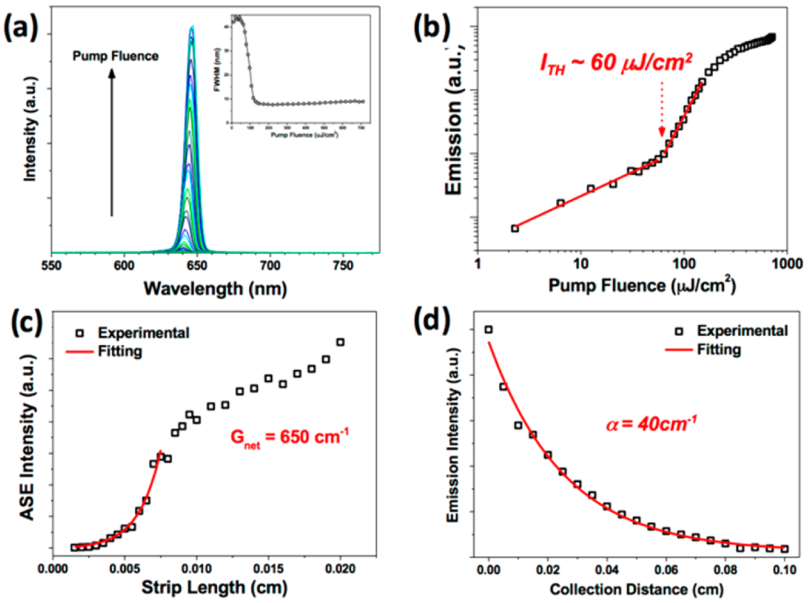

Figure 3. Optical characteristics of the DIAH-tethered QD film under pulsed excitation (440 nm, 5 ns pulse): (a) emission spectra from the DIAH-tethered QD film under different pumping energy density show the ASE and spectral narrowing (inset); (b) emission vs fluence behavior with an ASE threshold of ~60 $\mu J/cm^2$; (c) the VSL measurement shows an exponential increase in ASE intensity with longer pump strip lengths (pumped fluence of 500 $\mu J/cm^2$). Fitting the VSL curve yields a net gain value of 650 cm^{-1}. (d) An example of the experimental data and the fitting from an optical loss measurement for the low loss DIAH-tethered QD films.

much longer than the typical Auger recombination lifetime of 10−300 ps for Cd-based QDs (see below), we were able to observe clear signatures of ASE with increasing pump excitation intensity. The phenomena include spectral narrowing, the emergence of a red-shifted dominant emission band, and a clear threshold in the emission intensity vs excitation intensity plots (Figures 3a,b and S6d).

In fact, a significant spectral narrowing was seen as the pump fluence increased with the broad CW PL peak (a fwhm of ~45 nm) collapsing to a narrow ASE peak of ~8 nm fwhm (inset: Figure 3a). In addition, the ASE peak is positioned at 638 nm, which is red-shifted by ca. 9 nm with respect to the spontaneous PL peak position (~629 nm). The red-shift of ASE peak position may arise from the competition between optical gain from stimulated emission and optical loss from reabsorption in the single-exciton regime,[8] or due to the lower biexciton energies that result from attractive exciton−exciton interactions of type I-like QDs in the biexciton regime.[7] In addition to spectral narrowing and emission red-shifting, a threshold behavior was also observed in the emission intensity vs excitation intensity plots (Figure 3b). The nonlinear behavior is clearly evident from the abrupt increase of output intensity above the certain threshold. The significant spectral narrowing (5-fold) accompanies the exponential increase in emission intensity with the pump length which indicates lasing behavior (Figures 3c and S6c).

The DIAH-tethered QD film shows a minimum achievable threshold of approximately 44 $\mu J/cm^2$ (Figure S6b) and an average threshold of 60 ± 20 $\mu J/cm^2$ across different films and different spots on the same film. This threshold level is unusually low (an order of magnitude) in comparison to reported thresholds for common QD films such as CdSe/$Zn_{0.5}Cd_{0.5}S$ in the single-exciton regime (at 720 $\mu J/cm^2$), $CsPbBr_3$ perovskite QDs (at 450 $\mu J/cm^2$), and CdSe/CdS nanoplatelets (at 1000 $\mu J/cm^2$) which were also pumped using comparable sub-ns or ns lasers.[8,14]

We suggest that the unusually low ASE threshold of QD films fabricated here is a result of not only the properties of the QD film but also the system design. First, the utilization of large diameter QDs (~8.2 nm) with a large absorption cross-section increases the absorption of pump light.[22,53,54] We estimate the absorption cross-section of our CdSe/$Cd_{1-x}Zn_xSe_{1-y}S_y$ core/alloyed-shell QDs to be $\sigma \sim 10^{-14}$ cm^2 (based on the absorbance data of our cross-linked QD film), which is much larger than typical values of CdSe QDs that are usually around 10^{-15}−10^{-16} cm^2.[22,46] Second, highly reflective substrates (silicon, with a 290−295 nm thick SiO_2 surface layer) result in the excitation laser to pass twice through the film. Considering the reflection losses at the air/QD (~7%) and SiO_2/Si interfaces (reflectivity of Si is ~50%),[47] the overall effective pumping fluence is estimated to be 1.4 times (93% × 150%) of the input pumping fluence, which leads to a higher absorbed photon density in comparison to films deposited on transparent quartz substrates.[14,53] It is also noteworthy that the interference between incoming and reflected beams can occur due to the use of reflective substrate, leading to an intensity distribution with larger variation across the QD film region compared with the one without Si as the substrate (Figure S13). Finally, lower overall wave guide losses were obtained by introducing strong light confinement within the QD film due to the high index contrast between the QD film (n = 1.9) and the low-index supporting CYTOP layer (n = 1.34) (Figure 1a(iii)).

Further support for the low gain threshold observed in this system comes from the examination of the average number of excitons per QD, $\langle N \rangle$. This value can be calculated by considering the relationship $\langle N \rangle = f \times \sigma$, where f is the pump intensity and σ is the absorption cross-section.[22] This estimation gives $\langle N \rangle$ = 2 for a threshold of 84 $\mu J/cm^2$ (this value accounts for the double pass and reflection losses of the excitation laser through the QD film, 1.4 × 60 $\mu J/cm^2$). The average number of excitons per QD calculated here is much higher than that obtained for CdSe/$Zn_{0.5}Cd_{0.5}S$ QDs in the

DOI: 10.1021/acsphotonics.5b00743
ACS Photonics 2016, 3, 647−658

single-exciton regime ($\langle N \rangle$ = 0.86) and $CsPbBr_3$ perovskite QDs ($\langle N \rangle$ = 0.5−0.8).[8,14] This difference can be considered by taking into account the decay of excitons caused by Auger recombination that occurs during the long ns pump pulse duration.[8,14,48] When the 3.5 ns Auger recombination lifetime (measured from our QDs by transient absorption spectroscopy (Figure S5) is scaled with the 5 ns pulse width used in this study, the average number of excitons per QD is 1.1 ± 0.3. This value at the ASE threshold is in good agreement with values obtained in other low-threshold Cd-based core/shell QD systems.[22]

Net gain values as high as 650 cm^{-1} were obtained in the cross-linked QD films by fitting the ASE intensity versus the excitation length with the Malko model (under a pump intensity of 500 $\mu J/cm^2$), $I(L) = A_X L + B_{XX}/g_{net}(e^{g_{net}L} - 1)$, where A_X and B_{XX} are constants proportional to spontaneous emission intensity for excitons and biexcitons, L is the stripe length, and g_{net} is the net gain value.[25] This gain value is comparable to or higher than those of high gain CdSe nanoplatelets.[11−13] An average net gain value of 493 ± 106 cm^{-1} was obtained for multiple samples, different batches, and beam locations (Figure S6a). An average net gain value of 510 ± 110 cm^{-1} was found for highly loaded BA-capped QD films (Figure S7), which is very close to the DIAH cross-linked QD film and indicates that solid-state DIAH cross-linking does not significantly alter the optical gain of the QD film. These results can be explained by the fact that DIAH has the same functional group and length similar to that of BA molecules packed end-to-end. Thus, DIAH cross-linking does not significantly change the surface passivation, packing density, or optical properties during the solid-state exchange. However, the QD-QD linking provided by DIAH does impart chemical resistance and physical robustness to the films. In contrast, a much lower net gain value of 60 ± 20 cm^{-1} (and a higher average ASE threshold of 323 ± 66 $\mu J/cm^2$) were obtained from the long-chain OA-capped QD film which is the benchmark for common literature studies. Thus, the average net gain value for both QD films with short ligands (DIAH and BA in this work) is about an order of magnitude higher than that measured under identical conditions for low-density QD films with the long-chain OA ligand, indicating that the loading density, controlled by ligand shells, is critical.

Moreover, we compare current gain values in our study with those measured in the literature under different fabrication and pumping conditions (Figure 4a). The analysis shows a factor of up to 3-fold increase in comparison to values reported for a variety of drop-cast Cd-based QD films with different organic ligands (the literature reported gains of typically 60−200 cm^{-1}).[49,50] We suggest that the unusually high gain values observed in the QD solid films fabricated here are primarily due to the following major factors. First, the much higher QD loading of our films can effectively increase the material gain by 2-fold by considering the equation of modal gain, $g_{modal} = \Gamma \times g_{material}$,[32] where Γ is the modal confinement factor, and $g_{material}$ is the material gain. Second, the modal confinement factor can account for an additional 2-fold increase since the DIAH-QD films have a significantly higher refractive index contrast between the film and substrate than the OA-QD films (Figure S6e). Third, the passivation of the QD surface likely affects the optical gain magnitude by changing the rate and magnitude of surface trapping. In colloidal quantum dots, two major nonradiative pathways are surface trapping and Auger recombination.[6] In the past, Auger recombination was considered to dominate over surface trapping owing to the very fast Auger recombination lifetime of 1−100 ps. However, the Auger recombination lifetime in these CdSe/$Cd_{1-x}Zn_xSe_{1-y}S_y$ core/alloyed shell quantum dots is strongly suppressed (on the order of few ns), so we suggest that surface trapping related to poor passivation of the QD surface may be an important factor affecting optical gain.

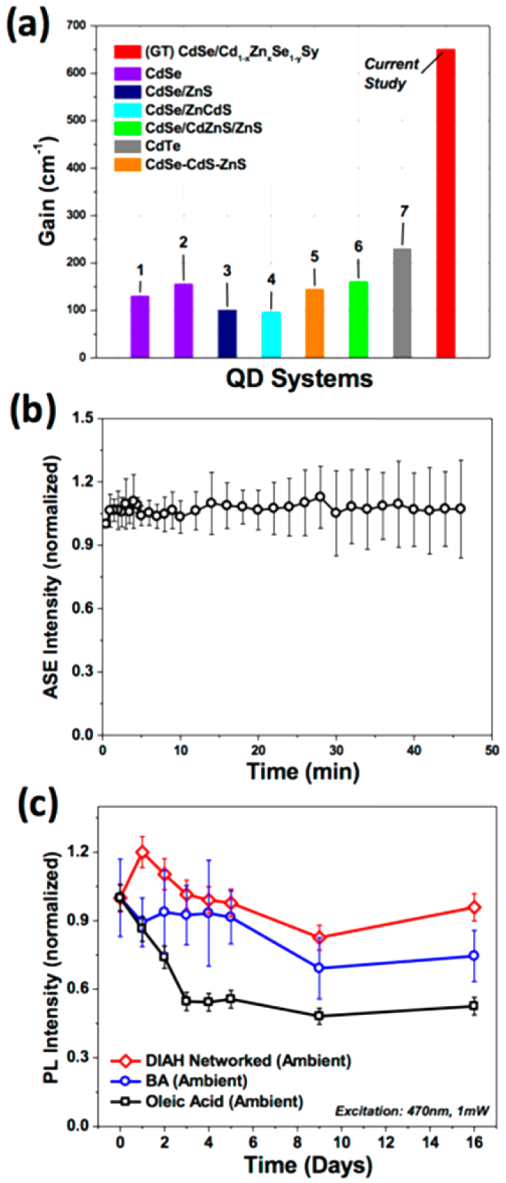

Figure 4. (a) Comparison of gain values observed in this study and in recent literature: 1, ref 51; 2, ref 25; 3, ref 52; 4, ref 8; 5, ref 53; 6, ref 24; 7, 54. (b) ASE stability tests of DIAH-tethered QD films pumped with 500 $\mu J/cm^2$ over 45 min of excitation. (c) CW PL stability tests of the DIAH-tethered QD film, BA-capped QD film, and OA-capped QD film under ambient conditions.

Indeed, the PL stability tests discussed in the next section show that both amine ligands (DIAH and BA) capping the QDs exhibit better PL stability compared to the carboxylic acid ligand (OA) capped QD films. This suggests that the amine group provides a more thorough and robust passivation of the QD surface compared to that of the OA ligands. Further study on how the chemical functionality of the QD ligands affects QD surface passivation (and the resulting optical gain) should be

DOI: 10.1021/acsphotonics.5b00743
ACS Photonics 2016, 3, 647−658

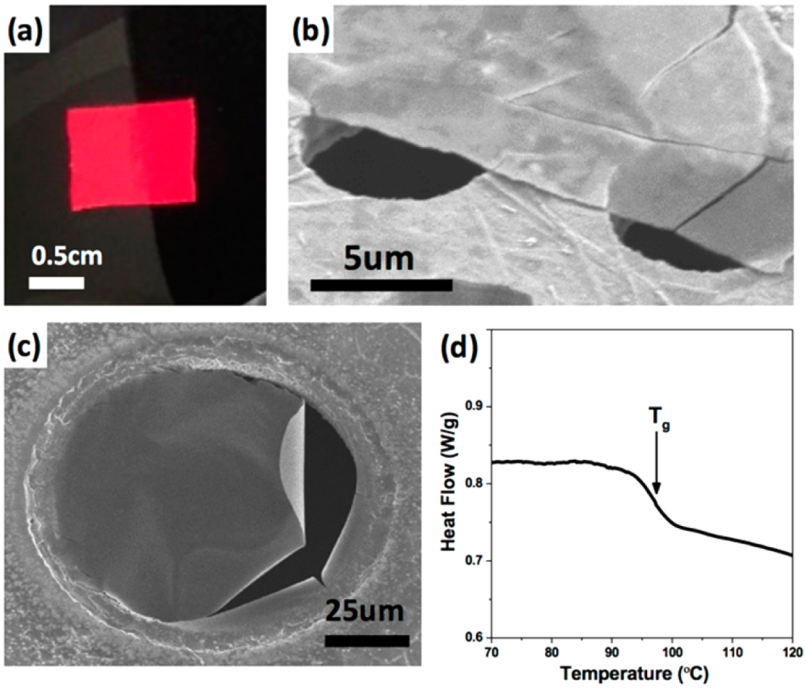

Figure 5. Physical and chemical stability of the cross-linked DIAH-tethered QD films and structures: (a) the carved film piece onto a new substrate; (b) the cross-linked QD film transferred onto a TEM grid with 7 μm holes and (c) 100 μm diameter holes (SEM images collected at an angle). (d) DSC of the DIAH cross-linked QD films with a glass transition near 97 °C (inset).

conducted in the future. Also, the much larger net gain value observed here may also be due in part to the high uniformity of the cross-linked QD films, which reduces optical scattering and leads to optical losses being as low as 50 cm^{-1} for some films (within the range of 40 cm^{-1} to 200 cm^{-1} for all films tested) (Figure S9).[55]

To further clarify the role of QD cross-linking with short bifunctional ligands, we conducted an ASE stability test under continuous optical pumping (Figure 4b). Remarkably, the ASE intensity of DIAH-passivated QD films remains constant during continuous pumping (500 $\mu J/cm^2$) over a period of 45 min (>25000 pulses, 10 Hz), indicating an excellent reproducibility over numerous laser shots within ±10%. This high stability is in sharp contrast to drop-cast CdSe nanoplatelet films that exhibit a reduction in intensity of up to 50% of the original value within 1 h, depending on the pumping intensity of the CW laser excitation.[10] Unfortunately, ASE stability tests were not reported for high performing gain materials of $CsPbX_3$ QDs.[14]

In addition to the ASE stability test, we performed long-term shelf lifetime PL stability by repeating PL measurements under identical conditions for samples stored under ambient conditions for an extended time (Figure 4c) (see also data for vacuum storage in Figure S8). These tests show that the cross-linked DIAH-tethered QD films display a long-term temporal stability of the PL intensity (within ±5% from the initial values). However, the PL intensity of non-cross-linked BA-capped QD films and traditional OA-capped QD films (widely reported in the literature) decayed dramatically within the same time period (50%−70% reduction of the original intensity) (Figure 4c). We suggest that the stronger binding affinity and higher surface coverage of QDs with shorter aliphatic amines provided a more thorough and robust passivation of the QD surface compared to that of the oleic acid ligands. The fast oxidation and diffusion of the conventional weakly bound ligands promote the generation of defect states on the QD surface that result in PL quenching.[36,56−58] Also, volatile aliphatic amines like BA that have a low m_p and b_p and a high vapor pressure can undergo desorption from the QD surface under ambient conditions, which further promotes a reduction of photoluminescence in uncross-linked short-ligand QD films.

Furthermore, to investigate the mechanical stability of cross-linked DIAH-ligand QD films, the films were released from the supporting silicon wafer substrate. After cutting a film piece they maintained their shape in the freely standing state. The films were then transferred onto TEM grids with openings from 7 to 100 μm (Figure 5b,c and Figure S9). This way, large cross-linked QD films (area >1 cm^2) can be transferred to different substrates while retaining structural integrity and film thickness (with occasional cracking), and composition (Figure S10). Thus, the cross-linked QD films can sustain harsh transfer processes (cutting, releasing, solvent treatment, and drying) in contrast to common drop-cast films which readily disintegrate even under mild rubbing.

Finally, in contrast to physically absorbed QD films reported to date, the cross-linked QD films also demonstrated superior chemical resistance to both polar and nonpolar solvents. This resistance facilitates the applicability of lithographical fabrication processes that require the deposition of different polymer resists and exposure to different solvent treatments. Indeed, consistent and well-defined QD patterns were fabricated by filling the square holes in a photoresist with QDs, removing the resist, and cross-linking the remaining QD squares (Figure S11). These patterns were found to maintain their initial shape after exposure to solvent washing and also through the deposition and removal of a polystyrene cladding layer (Figure 6).

DOI: 10.1021/acsphotonics.5b00743
ACS Photonics 2016, 3, 647−658

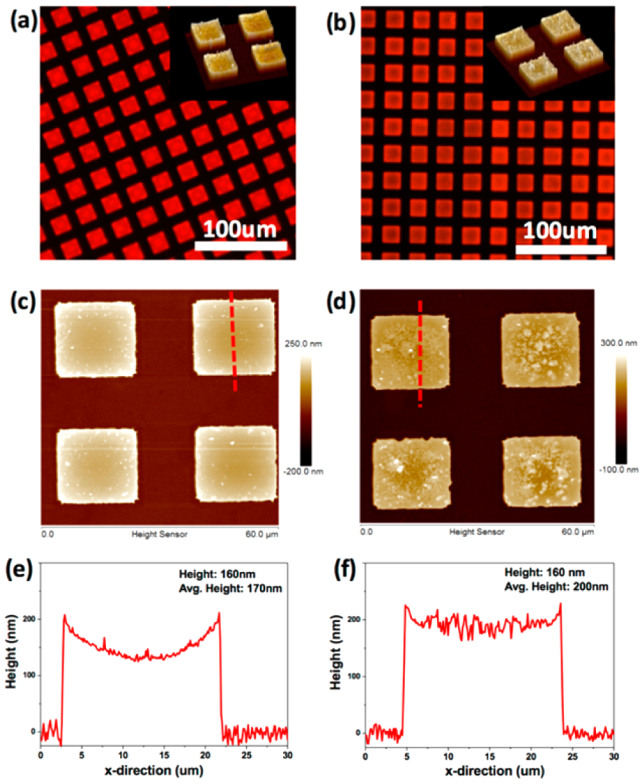

Figure 6. Optical microscopy images of (a) clean DIAH-tethered QD squares and (b) the squares after a polystyrene layer has been deposited and then removed. AFM scans of (c) height, (e) height cross-section for clean DIAH-tethered QD squares and (d) height, and (f) height cross-section for the squares after cladding/removal process. The DIAH-tethered QD patterned squares maintain their shape and size throughout and after the polymer cladding/removal process.

CONCLUSIONS

In summary, mechanically robust, optically stable, and highly loaded cross-linked core/alloyed-shell QD films with net gain values up to 650 cm^{-1} in the q-CW excitation region were successfully crafted by replacing commonly used long-chain organic ligands with short-chain bifunctional ligands with strong affinity to the QD surface. The net gain values reported here are much higher than those measured for long-chain oleic acid QD films and those reported for drop-cast QD films capped with various conventional organic ligands. The unusually low (an order of magnitude) ASE threshold observed here under ns pulse excitation can be utilized to generate significant optical gains under lower optical powers initiated by q-CW lasers. The cross-linking of uniformly distributed QDs imparts exceptional mechanical robustness, high chemical resistance, excellent thermal stability, and long-term optical stability, greatly outperforming conventional physically absorbed QD films passivated with traditional ligands.

We envision that the approach developed here can be extended to other promising gain media such as CdSe nanoplatelets and $CsPbX_3$ perovskite QDs that are typically capped with long ligands (i.e., oleic acid) due to the common synthetic routine. As the challenges of physical and PL instabilities of these materials are resolved, potentially by introduction of short functional highly bound ligands, large increases of net gain and enhanced stability can be expected. Furthermore, the robust cross-linking exploited in this study can be used to fabricate stable freestanding, optically active elements with well-defined dimensions that exhibit excellent chemical resistance. The demonstrated ability to photolithographically pattern QD films is of key importance for the fabrication of complex optical structures such as multicolor patterns (RGB pixels), responsive optical materials and metamaterials, sensing materials and structures, and parity-time-symmetric Bragg stacks where alternating gain/loss layers require multiple cycles of resist deposition/removal.[18,59−63] Moreover, QD structures with modulated optical gain and loss can be fabricated in the form of wave guides and other structures required for parity-time symmetric optical materials and other lasing metamaterials.[64,65]

MATERIALS AND METHODS

Chemicals and Materials. Cadmium oxide, tri-*n*-octylphosphine (TOP, 90%), and selenium powder were obtained from Sigma-Aldrich. 1-Tetradecylphosphonic acid (TDPA, 98%), tri-*n*-octylphosphine oxide (TOPO, 90%), diethylzinc (15 weight% in hexane), and hexane were obtained from Alfa Aesar. 1-Octadecene (ODE, 90%), hexadecylamine (HDA, 90%), butylamine (BA, 98%), oleic acid (OA, 97%), and bis(trimethylsilyl) sulfide (95%) were obtained from TCI. 1,7 Diaminoheptane (DIAH, 98%) and ethyl lactate were obtained from Sigma-Aldrich. Toluene and heptane were obtained from BDH Chemicals. CYTOP was from obtained AGC Chemicals. All chemicals were used as received.

Synthesis of Compositional Gradient CdSe/$Cd_{1-x}Zn_xSe_{1-y}S_y$ QDs. Chemical composition gradient CdSe/$Cd_{1-x}Zn_xSe_{1-y}S_y$ core/alloyed-shell QDs were synthesized by modifying a reported method.[38,66] Briefly, 0.2 mmol of CdO, 4 mmol of $Zn(acetate)_2$, 5 mL of oleic acid, and 15 mL of 1-octadecene (ODE) were placed in a three-necked flask and degassed at 150 °C for 1 h. The reaction was heated to 300 °C under Ar. At the elevated temperature (300 °C), 1 mmol of Se and 4 mmol of S in 2 mL of TOP were rapidly injected into the reaction vessel. The reaction was allowed to proceed at 300 °C for 10 min, and then the heating mantle was removed to stop the reaction. Five milliliters of hexane was added to the solution once the temperature reached 70 °C.

Ligand Exchange. The oleic acid-capped CdSe/$Cd_{1-x}Zn_xSe_{1-y}S_y$ QDs were centrifuged with acetone three times to remove excess oleic acid and ODE. Subsequently, purified oleic acid-capped CdSe/$Cd_{1-x}Zn_xSe_{1-y}S_y$ QDs were redispersed in hexane, and an excess amount of butylamine was added to perform the solution-phase ligand exchange. The ligand exchange reaction was allowed to proceed at 45 °C for 1 day. The solution was then precipitated using methanol and redispersed in a mixture of hexane and an excess amount of BA. This procedure was repeated three times. Upon ligand replacement, the QD film loading (as determined by refractive index) (Table S2) increased from 27% to 53% in the BA-capped QD films, a nearly 2-fold increase. This is an extremely high loading of QD considering that the loading of ideal spherical particles without capping ligands ranges from 52% for simple cubic to 74% for face centered cubic arrangements. The choice to use DIAH as the bifunctional cross-linker following ligand exchange can be rationalized as follows. First, the length of a bifunctional cross-linker needs to be carefully chosen so that it can effectively replace the capping ligand BA during the solid-state exchange. In an ideal case, where BAs are fully extended when capping the QD surface, the gaps between QDs is the length of two BA molecules (eight C−C bonds). Thus, an appropriate bifunctional cross-linker should be shorter in

DOI: 10.1021/acsphotonics.5b00743
ACS Photonics 2016, 3, 647−658

order to efficiently fill the gaps between QDs without compromising their close packing.

The solid-state exchange is performed by soaking the prepared butylamine-capped QD films in a 0.1 M methanol solution of 1,7 diaminoheptane for 1 h. After soaking, the films are washed with methanol 3 times to remove any excess 1,7 diaminoheptane. Notably, after ligand exchange, the film is rendered insoluble in both polar and nonpolar solvents, indicating successful cross-linking treatment by DIAH (Figure S1). It was observed that the QD loading did not significantly change during the networking step (53% to 49%), which may be due to the similar lengths of two BA ligands and the length of one DIAH ligand if the ligands are fully extended between adjacent QD surfaces.

Film Preparation. QD films were fabricated by spin-coating a QD heptane solution of ~60 mg/mL at 1000 rpm for 1 min. The film thickness ranged from 150 to 250 nm in order to support only the first waveguide mode. The QD films were deposited on CYTOP (AGC Chemicals) coating, which has a sufficiently low refractive index (n_{650} = 1.34) to provide light confinement and wave guiding within the QD film. The CYTOP was exposed to air or Ar plasma for 5 s in order to improve the wetting of CYTOP by QDs. Silicon, with a 290−295 nm thick SiO_2 surface layer, was used as a substrate since its large extinction coefficient attenuates much of the light that leaks into the substrate. The attenuation of light that leaks from the QD film into the Si substrate ensures that the light detected at the edge is the light that has propagated through the QD film. The substrate was cleaved to obtain sharper, cleaner edges to improve the intensity of the output light and ensure that the area of the film exposed to the pump light was uniform over the length of the pump strip length.

Fourier Transform Infrared Spectroscopy. ATR-FTIR measurements of cross-linked and noncross-linked QD films were conducted using a Bruker FTIR spectrometer Vertex 70 equipped with a narrow-band mercury cadmium telluride detector in accordance with a procedure described previously.[67] Noncross-linked QD films were deposited on the silica crystal by spin coating 30 μL of a butylamine (BA)-capped QD heptane solution at 1000 rpm for 1 min. After the measurement of noncross-linked QD films, the as-deposited film was soaked in a 0.1 M methanol solution of 1,7 diaminoheptane (DIAH) to perform the solid-state ligand exchange. FTIR spectra were collected in the range of 4000−900 cm^{-1} with a resolution 1 cm^{-1}. An accumulation of 10 scans was analyzed to confirm the successful chemical transformation.

The asymmetric and symmetric CH_3 stretching (2958 and 2854 cm^{-1}) decreased significantly during the solid-state ligand exchange, indicating a chemical composition associated with a cross-linking reaction (Figure S5c and Table S3). The ratio of asymmetric CH_3/CH_2 peaks dropped from 0.33 to 0.07, a 79% reduction, while the ratio of symmetric CH_3/CH_2 peaks decreased from 0.739 to 0.243, a 66% reduction. The large reduction of CH_3 intensity in both asymmetric and symmetric CH_3 stretching indicates that a substantial amount of BA was replaced by DIAH. In addition, the N−H stretching band remained similar during the solid-state ligand exchange process, with two peaks assigned to be the symmetric N−H stretching of 3324 cm^{-1} and the shoulder band of 3133 cm^{-1} (Figure S5b). The absence of the asymmetric N−H stretching peak may be due to the formation of a coordination bond on the QD surface that suppresses the asymmetric N−H stretching usually observed around 3300−3500 cm^{-1}.[68] The lack of asymmetric N−H stretching also suggests that the amino group on each end of DIAH is successfully bound to the QD surface.

Variable Stripe Length Measurement. The third harmonic (355 nm) of a Spectra Physics Quanta-Ray INDI-series Pulsed Nd:YAG laser (pulse width of 5−8 ns, repetition rate of 10 Hz) was used directly as a seed for a GWU-Lasertechnik basiScan Beta-Barium Borate Optical Parametric Oscillator, producing tunable pulses of 440 with a 25 mJ maximum pulse power (pulse width of 3−7 ns). For the variable stripe length (VSL) gain measurements,[45] the excitation beam was shaped into a stripe of 125 μm width using a cylindrical lens (15 cm focus length), and the stripe length was controlled by a pair of blades mounted on mechanically controlled stages that provided an adjustable slit. Only the central 10% of the beam was used to minimize pump inhomogeneity due the Gaussian intensity profile. The pump beam intensity, I_{pump}, was varied by means of a pair of polarizers. One end of the stripe excitation was placed on the cleaved edge of the film, while the length of the excitation stripe was progressively increased.

The emission from the edge was collected with a 1 mm diameter fiber and recorded using a commercial spectrometer (Ocean Optics USB4000; resolution 2 nm). Gain values were extracted according to the model proposed by Malko et al.[25] Loss measurements were conducted in the same experimental geometry. In this case, the length of the excitation stripe was held constant, while the distance of the stripe from the edge of the film, d, was varied by simultaneously varying the position of both blades. As the emission propagates toward the collecting fiber, it experiences attenuation by scattering and reabsorption from the unexcited region of the film. The decay of the collected emission signal with increasing distance from the edge was fit to an exponential $I(d) = I(0)\exp(-\alpha d)$ to extract the loss coefficient α.

Calculation of Confinement Factor. The confinement factor was calculated using Lumerical Mode Solutions. The model was based on the real QD system, with a stack of 5 layers: Si (3 μm)/SiO_2(292 nm)/CYTOP(1.5 μm)/QD(varied thickness)/air(5 μm). The power confined in the QD layer was integrated by using the option of power and intensity integration. The confinement factor was defined as $\Gamma = \int_0^t |E_x^2| dy / \int_{-\infty}^{\infty} |E_x^2| dy$, where t is the thickness of the QD layer.

Optical Characterization. UV−vis extinction spectra of QD solutions (quartz cuvette) from 350 to 900 nm (1 nm intervals) were collected using a Shimadzu UV−vis-2450 spectrometer with D2 and tungsten lamps offering a wavelength range of 300−1100 nm. The QD extinction spectra were corrected against the pure solvent background and the same quartz cuvette. Photoluminescence spectra of QD solutions were collected using a Shimadzu fluorescent RF-5301PC spectrofluorophotometer with the excitation wavelength of 525 nm.

Photoluminescence (PL) images were collected using a Dagexcel-M Digital Firewire camera (cooled). All PL imaging was performed using photoluminescence excitation from a blue bandpass filter (450−490 nm) with a dichroic mirror that reflects optical wavelengths below 495 nm, and with a long-pass emission filter that passes optical wavelengths above 500 nm. The light source is a quartz halogen lamp with an aluminum reflector providing a wavelength range of 420−850 nm and a power of 150 W of nonpolarized light.

PL Stability Measurement. PL from QD films were collected from hyperspectral data cubes. Hyperspectral data

DOI: 10.1021/acsphotonics.5b00743
ACS Photonics 2016, 3, 647−658

cubes were collected using a CytoViva hyperspectral imaging system utilizing a diffraction grating spectrophotometer with a spectral range of 400−1000 nm and a spectral resolution of 2.8 nm. A 10× objective (NA: 0.30) was used to scan the surface with scans of 50 lines with an automated stage (10 nm step size scan resolution). A 0.1 s exposure time (per line) was used. Hyperspectral scans were performed using the blue bandpass filter (450−490 nm) excitation setup. The light source was the quartz halogen lamp with an aluminum reflector. Spectra were collected and averaged from hundreds of points on the sample. The lamp power was set to 1 mW for all measurements.

Quantum Yield Measurement. Quantum yields of QDs dispersed in chloroform are determined by the relative quantum yield method developed in literature.[69] A standard sample, rhodamine 101 (QY = 91.5%), dissolved in ethanol was used to determine QDs emitting at red regions. UV−vis extinction spectra of QD solutions (quartz cuvette) from 350 to 900 nm (1 nm intervals) were collected using a Shimadzu UV−vis-2450 spectrometer with D2 and tungsten lamps offering a wavelength range of 300−1100 nm. The QD extinction spectra were corrected against the pure solvent background and the same quartz cuvette. Photoluminescence spectra of QD solutions were collected using a Shimadzu fluorescent RF-5301PC spectrofluorophotometer with the excitation wavelengths of 525 nm. All of the extinction values of solutions are diluted to be less than 0.1 before measurement in order to avoid the reabsorption effect.

fs-Transient Absorption. Pump−probe transient absorption spectroscopy was measured using a homemade Ti:sapphire laser oscillator operating at a 1 kHz repetition rate at 800 nm of 150 fs pulse duration. The laser beam was split into two beams. One beam was subsequently frequency doubled to 400 nm with a pulse energy of 10 μJ using a $BaBO_2$ nonlinear crystal and used to pump the sample, while the other was used to generate a white light supercontinuum with an energy range of 1.15 to 2.7 eV to serve as the probe beam. The pump and probe beams were carefully adjusted to obtain a complete spatial overlap. The transmission of the probe beam, T, is measured by a photodiode after dispersion by a monochromator in the absence of the pump and at various time delays after the pump arrives at the sample, yielding the normalized pump-induced change in transmission, $\Delta T(\lambda,t)/T$.

Ellipsometer and Determination of QD Loading. The QD films were examined using a spectroscopic ellipsometer from Woollam (model M2000) with a wavelength range of 245−1000 nm and a rotating compensator configuration. Film thickness was determined by applying a Cauchy model to the transparent region of the optical spectrum. The refractive index at 650 nm (also in the transparent region) was estimated using the Cauchy model. QD-loading (volume fraction) was determined by applying the effective medium approximation Bruggeman model to the refractive index at 650 nm to fit for the volume fraction of QDs in the film (with thickness treated as a constant). The refractive index of $CdSe/Cd_{1-x}Zn_xSe_{1-y}S_y$ QD was approximated using the refractive index of bulk CdSe (n_{bulk} = 2.4), and the refractive index value of the ligand at 650 nm was adjusted according to the ligand content.[37]

Fabrication of QD Patterns. The negative resist NR71-3000p was diluted by adding ethyl lactate to one-third of the original concentration of the solution provided by the company. The diluted resist was spin-cast on the silicon substrate (3000 rpm for 1 min). The cast film was subsequently soft baked at 165 °C for 5 min and exposed to 365 nm with a dosage of 252 mW/μm. The exposed film was then postbaked at 100 °C for 5 min and developed by soaking in the RD6 developer for 30 s. After development, the film was rinsed with water and dried by blowing with air. The QD patterns were fabricated by spin-casting the QD solution (in heptane) of ∼60 mg/mL at 1000 rpm for 1 min onto the polymer pattern. The polymer pattern is subsequently removed by soaking in acetone. A layer of polystyrene was deposited on the QD pattern by spin-coating a 12% toluene solution (3000 rpm, 1 min). The PS film was subsequently removed by washing at least three times with toluene until the original color of the film returned.

Film Transfer Process. The cross-linked film with a thickness of 80−85 nm was prepared via the procedure described above. Different concentrations of polystyrene solution were spin-cast on the cross-linked film to form a thickness near 1 μm (silicon substrate) and 150 nm (TEM grid). The prepared film was cut to remove the edges or to form smaller pieces and subsequently peeled off at the water interface. The silicon substrate/TEM grid was then immersed in water and used to pick up the prepared film. After the film is dried, toluene was used to rinse the film at least 3 times until the polystyrene layer was removed and the original color of the DIAH-tethered QD film appeared again.

Atomic Force Microscopy. AFM images were collected using a Dimension Icon AFM microscope (Bruker) in tapping mode according to the usual procedure.[67] MikroMasch pyramidal silicon tips were used with a height of 15 μm, a cantilever length of 150 μm, and a spring constant of 7 N/m. Scan size ranged from 50 μm by 50 μm to 500 nm by 500 nm with a scan rate within 0.3−0.8 Hz.[70]

Differential Scanning Calorimeter. The heat flow as a function of temperature of the DIAH-tethered QD sample was measured using a TA Instruments DSC (differential scanning calorimeter) Q200 with hermitically sealed aluminum pans. Samples were analyzed from −50 to 200 °C using a 10 °C/min temperature profile under a constant flow of argon.

Transmission Electron Microscopy (TEM). The interparticle distance of $CdSe/Cd_{1-x}Zn_xSe_{1-y}S_y$ QDs was studied using a high-resolution transmission electron microscope (Tecnai F30). An accelerating voltage of 300 keV was used. TEM samples were prepared by diluting the original QD solution of ∼6 mg/mL 30 times. Then, 5−10 μL of the diluted solution was drop-cast on the TEM grid and allowed to dry completely. The DIAH-tethered QD sample was prepared by making the BA-capped QD sample and then subsequently performing the cross-linking process for 1 h.

Scanning Electron Microscopy. SEM characterization was performed on a Hitachi S-3400N SEM with a back scattering electron detector with an accelerating voltage in the range 2−5 kV.

■ ASSOCIATED CONTENT

Supporting Information

The Supporting Information is available free of charge on the ACS Publications website at DOI: 10.1021/acsphotonics.5b00743.

(1) Thermodynamic properties and refractive index of ligand; (2) refractive index and QD loading of films; (3) optical properties of OA and BA capped QD in chloroform; (4) figure of chemical resistance enabled by cross-linking process; (5) TEM/AFM/FTIR/bright

DOI: 10.1021/acsphotonics.5b00743
ACS Photonics 2016, 3, 647−658

field/dark field/fluorescence images of OA, BA, and DIAH-QD films/structures; (6) transient absorption of the QD film; (7) ASE threshold/VSL measurements of BA and DIAH-QD films; (8) thickness dependent confinement factor of OA and DIAH-QD films; (9) PL stability tests of BA and DIAH-QD films stored under vacuum; and (10) intensity distributions of the pumping laser in the thin film with and without Si as the substrate (PDF)

AUTHOR INFORMATION

Corresponding Author

*E-mail: Vladimir@mse.gatech.edu.

Notes

The authors declare no competing financial interest.

ACKNOWLEDGMENTS

Financial support is acknowledged from the Air Force Office of Scientific Research FA9550-14-1-0037 (Synthetic Photonics Multidisciplinary University Research Initiative), the National Science Foundation (ECCS-1305087), and the UES-AFRL support S-977-022-001. M.J.S. would like to acknowledge the Science, Mathematics and Research for Transformation (SMART) scholarship funded by OSD-T&E (Office of Secretary Defense-Test and Evaluation), Defense-Wide/PE0601120D8Z National Defense Education Program (NDEP)/BA-1, Basic Research, and SMART Program office Grant Number N00244-09-1-0081.

REFERENCES

(1) Murray, C. B.; Norris, D. J.; Bawendi, M. G. Synthesis and characterization of nearly monodisperse CdE (E = S, Se, Te) Semiconductor nanocrystallites. *J. Am. Chem. Soc.* **1993**, *115*, 8706−8715.

(2) Zimnitsky, D.; Jiang, C.; Xu, J.; Lin, Z.; Tsukruk, V. V. Substrate- and Time-Dependent Photoluminescence of Quantum Dots Inside the Ultrathin Polymer LbL Film. *Langmuir* **2007**, *23*, 4509−4515.

(3) Zimnitsky, D.; Jiang, C.; Xu, J.; Lin, Z.; Zhang, L.; Tsukruk, V. V. Photoluminescence of a Freely Suspended Monolayer of Quantum Dots Encapsulated into Layer-by-Layer Films. *Langmuir* **2007**, *23*, 10176−10183.

(4) Xu, J.; Wang, J.; Mitchell, M.; Mukherjee, P.; Jeffries-El, M.; Petrich, J. W.; Lin, Z. Organic−Inorganic Nanocomposites via Directly Grafting Conjugated Polymers onto Quantum Dots. *J. Am. Chem. Soc.* **2007**, *129*, 12828−12833.

(5) Zhao, L.; Lin, Z. Crafting Semiconductor Organic−Inorganic Nanocomposites via Placing Conjugated Polymers in Intimate Contact with Nanocrystals for Hybrid Solar Cells. *Adv. Mater.* **2012**, *24*, 4353−4368.

(6) Klimov, V. I.; Mikhailovsky, A. A.; Xu, S.; Malko, A.; Hollingsworth, J. A.; Leatherdale, C. A.; Eisler, H. J.; Bawendi, M. G. Optical gain and stimulated emission in nanocrystal quantum dots. *Science* **2000**, *290*, 314−317.

(7) Klimov, V. I.; Ivanov, S. A.; Nanda, J.; Achermann, M.; Bezel, I.; McGuire, J. A.; Piryatinski, A. Single-exciton optical gain in semiconductor nanocrystals. *Nature* **2007**, *447*, 441−446.

(8) Dang, C.; Lee, J.; Breen, C.; Steckel, J. S.; Coe-Sullivan, S.; Nurmikko, A. Red, green and blue lasing enabled by single-exciton gain in colloidal quantum dot films. *Nat. Nanotechnol.* **2012**, *7*, 335−339.

(9) Schaller, R. D.; Petruska, M. A.; Klimov, V. I. Tunable near-infrared optical gain and amplified spontaneous emission using PbSe nanocrystals. *J. Phys. Chem. B* **2003**, *107*, 13765−13768.

(10) Grim, J. Q.; Christodoulou, S.; Di Stasio, F.; Krahne, R.; Cingolani, R.; Manna, L.; Moreels, I. Continuous-wave biexciton lasing at room temperature using solution-processed quantum wells. *Nat. Nanotechnol.* **2014**, *9*, 891−895.

(11) Guzelturk, B.; Kelestemur, Y.; Olutas, M.; Delikanli, S.; Demir, H. V. Amplified Spontaneous Emission and Lasing in Colloidal Nanoplatelets. *ACS Nano* **2014**, *8*, 6599−6605.

(12) She, C.; Fedin, I.; Dolzhnikov, D. S.; Dahlberg, P. D.; Engel, G. S.; Schaller, R. D.; Talapin, D. V. Red, Yellow, Green, and Blue Amplified Spontaneous Emission and Lasing Using Colloidal CdSe Nanoplatelets. *ACS Nano* **2015**, *9*, 9475−9485.

(13) She, C. X.; Fedin, I.; Dolzhnikov, D. S.; Demortiere, A.; Schaller, R. D.; Pelton, M.; Talapin, D. V. Low-Threshold Stimulated Emission Using Colloidal Quantum Wells. *Nano Lett.* **2014**, *14*, 2772−2777.

(14) Yakunin, S.; Protesescu, L.; Krieg, F.; Bodnarchuk, M. I.; Nedelcu, G.; Humer, M.; De Luca, G.; Fiebig, M.; Heiss, W.; Kovalenko, M. V. Low-threshold amplified spontaneous emission and lasing from colloidal nanocrystals of caesium lead halide perovskites. *Nat. Commun.* **2015**, *6*, 8056−8056.

(15) Hodaei, H.; Miri, M.-A.; Heinrich, M.; Christodoulides, D. N.; Khajavikhan, M. Parity-time−symmetric microring lasers. *Science* **2014**, *346*, 975−978.

(16) Feng, L.; Wong, Z. J.; Ma, R.-M.; Wang, Y.; Zhang, X. Single-mode laser by parity-time symmetry breaking. *Science* **2014**, *346*, 972−975.

(17) Makris, K. G.; El-Ganainy, R.; Christodoulides, D. N.; Musslimani, Z. H. Beam dynamics in *PT* symmetric optical lattices. *Phys. Rev. Lett.* **2008**, *100*, 103904.

(18) Lin, Z.; Ramezani, H.; Eichelkraut, T.; Kottos, T.; Cao, H.; Christodoulides, D. N. Unidirectional Invisibility Induced by *PT*-Symmetric Periodic Structures. *Phys. Rev. Lett.* **2011**, *106*, 213901.

(19) Chang, L.; Jiang, X. S.; Hua, S. Y.; Yang, C.; Wen, J. M.; Jiang, L.; Li, G. Y.; Wang, G. Z.; Xiao, M. Parity-time symmetry and variable optical isolation in active-passive-coupled microresonators. *Nat. Photonics* **2014**, *8*, 524−529.

(20) Guzelturk, B.; Erdem, O.; Olutas, M.; Kelestemur, Y.; Demir, H. V. Stacking in Colloidal Nanoplatelets: Tuning Excitonic Properties. *ACS Nano* **2014**, *8*, 12524−12533.

(21) Park, Y.-S.; Guo, S.; Makarov, N. S.; Klimov, V. I. Room Temperature Single-Photon Emission from Individual Perovskite Quantum Dots. *ACS Nano* **2015**, *9*, 10386−10393.

(22) Guzelturk, B.; Kelestemur, Y.; Gungor, K.; Yeltik, A.; Akgul, M. Z.; Wang, Y.; Chen, R.; Dang, C.; Sun, H.; Demir, H. V. Stable and Low-Threshold Optical Gain in CdSe/CdS Quantum Dots: An All-Colloidal Frequency Up-Converted Laser. *Adv. Mater.* **2015**, *27*, 2741−2746.

(23) Malak, S. T.; Jung, J.; Yoon, Y. J.; Smith, M. J.; Lin, C. H.; Lin, Z.; Tsukruk, V. V. Large-area multicolor patterning of quantum dot-polymer films via targeted recovery of emission signature. *Adv. Opt. Mater.* **2016**, DOI: 10.1002/adom.201500670.

(24) Todescato, F.; Fortunati, I.; Gardin, S.; Garbin, E.; Collini, E.; Bozio, R.; Jasieniak, J. J.; Della Giustina, G.; Brusatin, G.; Toffanin, S.; Signorini, R. Soft-Lithographed Up-Converted Distributed Feedback Visible Lasers Based on CdSe-CdZnS-ZnS Quantum Dots. *Adv. Funct. Mater.* **2012**, *22*, 337−344.

(25) Malko, A. V.; Mikhailovsky, A. A.; Petruska, M. A.; Hollingsworth, J. A.; Htoon, H.; Bawendi, M. G.; Klimov, V. I. From amplified spontaneous emission to microring lasing using nanocrystal quantum dot solids. *Appl. Phys. Lett.* **2002**, *81*, 1303−1305.

(26) Hoogland, S.; Sukhovatkin, V.; Howard, I.; Cauchi, S.; Levina, L.; Sargent, E. H. A solution-processed 1.53 μm quantum dot laser with temperature-invariant emission wavelength. *Opt. Express* **2006**, *14*, 3273−3281.

(27) Sukhovatkin, V.; Musikhin, S.; Gorelikov, I.; Cauchi, S.; Bakueva, L.; Kumacheva, E.; Sargent, E. H. Room-temperature amplified spontaneous emission at 1300 nm in solution-processed PbS quantum-dot films. *Opt. Lett.* **2005**, *30*, 171−173.

(28) Koleilat, G. I.; Levina, L.; Shukla, H.; Myrskog, S. H.; Hinds, S.; Pattantyus-Abraham, A. G.; Sargent, E. H. Efficient, Stable Infrared Photovoltaics Based on Solution-Cast Colloidal Quantum Dots. *ACS Nano* **2008**, *2*, 833−840.

DOI: 10.1021/acsphotonics.5b00743
ACS Photonics 2016, 3, 647−658

(29) Luther, J. M.; Law, M.; Song, Q.; Perkins, C. L.; Beard, M. C.; Nozik, A. J. *ACS Nano* **2008**, *2*, 271−280.
(30) Zhao, N.; Osedach, T. P.; Chang, L.-Y.; Geyer, S. M.; Wanger, D.; Binda, M. T.; Arango, A. C.; Bawendi, M. G.; Bulovic, V. Colloidal PbS Quantum Dot Solar Cells with High Fill Factor. *ACS Nano* **2010**, *4*, 3743−3752.
(31) Zarghami, M. H.; Liu, Y.; Gibbs, M.; Gebremichael, E.; Webster, C.; Law, M. Structural, Optical, and Electrical Properties of Self-Assembled Films of PbSe Nanocrystals Treated with 1,2-Ethanedithiol. *ACS Nano* **2010**, *4*, 2475−2485.
(32) Adachi, M. M.; Fan, F.; Sellan, D. P.; Hoogland, S.; Voznyy, O.; Houtepen, A. J.; Parrish, K. D.; Kanjanaboos, P.; Malen, J. A.; Sargent, E. H. Microsecond-sustained lasing from colloidal quantum dot solids. *Nat. Commun.* **2015**, *6*.
(33) Kowalczyk, B.; Apodaca, M. M.; Nakanishi, H.; Smoukov, S. K.; Grzybowski, B. A. Lift-Off and Micropatterning of Mono- and Multilayer Nanoparticle Films. *Small* **2009**, *5*, 1970−1973.
(34) Schlicke, H.; Battista, D.; Kunze, S.; Schröter, C. J.; Eich, M.; Vossmeyer, T. Freestanding Membranes of Cross-Linked Gold Nanoparticles: Novel Functional Materials for Electrostatic Actuators. *ACS Appl. Mater. Interfaces* **2015**, *7*, 15123−15128.
(35) Wuister, S. F.; de Mello Donegá, C.; Meijerink, A. Influence of Thiol Capping on the Exciton Luminescence and Decay Kinetics of CdTe and CdSe Quantum Dots. *J. Phys. Chem. B* **2004**, *108*, 17393−17397.
(36) Hines, D. A.; Kamat, P. V. Recent Advances in Quantum Dot Surface Chemistry. *ACS Appl. Mater. Interfaces* **2014**, *6*, 3041−3057.
(37) Sigma-Aldrich. Butylamine, 1,7 diaminoheptane, & oleic acid.
(38) Bae, W. K.; Char, K.; Hur, H.; Lee, S. Single-Step Synthesis of Quantum Dots with Chemical Composition Gradients. *Chem. Mater.* **2008**, *20*, 531−539.
(39) Xu, F.; Gerlein, L. F.; Ma, X.; Haughn, C. R.; Doty, M. F.; Cloutier, S. G. Impact of Different Surface Ligands on the Optical Properties of PbS Quantum Dot Solids. *Materials* **2015**, *8*, 1858−1870.
(40) Kagan, C. R.; Murray, C. B.; Bawendi, M. G. Long-range resonance transfer of electronic excitations in close-packed CdSe quantum-dot solids. *Phys. Rev. B: Condens. Matter Mater. Phys.* **1996**, *54*, 8633−8643.
(41) Wood, V.; Panzer, M. J.; Caruge, J.-M.; Halpert, J. E.; Bawendi, M. G.; Bulović, V. Air-Stable Operation of Transparent, Colloidal Quantum Dot Based LEDs with a Unipolar Device Architecture. *Nano Lett.* **2010**, *10*, 24−29.
(42) Beck, K. R.; Korsmeyer, R.; Kunz, R. J. An overview of the glass transition temperature of synthetic polymers. *J. Chem. Educ.* **1984**, *61*, 668.
(43) Socrates, G. *Infrared and Raman Characteristic Group Frequencies: Tables and Charts*; John Wiley & Sons, Ltd.: Chichester, England, 2001.
(44) Marshall, C. P.; Javaux, E. J.; Knoll, A. H.; Walter, M. R. Combined micro-Fourier transform infrared (FTIR) spectroscopy and micro-Raman spectroscopy of Proterozoic acritarchs: A new approach to Palaeobiology. *Precambrian Res.* **2005**, *138*, 208−224.
(45) Shaklee, K. L.; Leheny, R. F. Direct determination of optical gain in semiconductor crystals. *Appl. Phys. Lett.* **1971**, *18*, 475−477.
(46) Chen, O.; Zhao, J.; Chauhan, V. P.; Cui, J.; Wong, C.; Harris, D. K.; Wei, H.; Han, H.-S.; Fukumura, D.; Jain, R. K.; Bawendi, M. G. Compact high-quality CdSe−CdS core−shell nanocrystals with narrow emission linewidths and suppressed blinking. *Nat. Mater.* **2013**, *12*, 445−451.
(47) Green, M. A. Self-consistent optical parameters of intrinsic silicon at 300 K including temperature coefficients. *Sol. Energy Mater. Sol. Cells* **2008**, *92*, 1305−1310.
(48) Lampert, Z. E.; Lappi, S. E.; Papanikolas, J. M.; Lewis Reynolds, C. Intrinsic optical gain in thin films of a conjugated polymer under picosecond excitation. *Appl. Phys. Lett.* **2013**, *103*, 033303.
(49) Guzelturk, B.; Kelestemur, Y.; Akgul, M. Z.; Sharma, V. K.; Demir, H. V. Ultralow Threshold One-Photon- and Two-Photon-Pumped Optical Gain Media of Blue-Emitting Colloidal Quantum Dot Films. *J. Phys. Chem. Lett.* **2014**, *5*, 2214−2218.
(50) Wang, Y.; Yang, S.; Yang, H.; Sun, H. Quaternary Alloy Quantum Dots: Toward Low-Threshold Stimulated Emission and All-Solution-Processed Lasers in the Green Region. *Adv. Opt. Mater.* **2015**, *3*, 652−657.
(51) Petruska, M. A.; Malko, A. V.; Voyles, P. M.; Klimov, V. I. High-performance, quantum dot nanocomposites for nonlinear optical and optical gain applications. *Adv. Mater.* **2003**, *15*, 610−613.
(52) Chan, Y.; Steckel, J. S.; Snee, P. T.; Caruge, J. M.; Hodgkiss, J. M.; Nocera, D. G.; Bawendi, M. G. Blue semiconductor nanocrystal laser. *Appl. Phys. Lett.* **2005**, *86*, 073102.
(53) Jasieniak, J.; Fortunati, I.; Gardin, S.; Signori, R.; Bozio, R.; Martucci, A.; Mulvaney, P. Highly Efficient Amplified Stimulated Emissionfrom CdSe-CdS-ZnS Quantum Dot Doped Wavequides with Two-Photon Infrared Optical Pumping. *Adv. Mater.* **2008**, *20*, 69−73.
(54) Roither, J.; Pichler, S.; Kovalenko, M. V.; Heiss, W.; Feychuk, P.; Panchuk, O.; Allam, J.; Murdin, B. N. Two- and one-dimensional light propagations and gain in layer-by-layer-deposited colloidal nanocrystal waveguides. *Appl. Phys. Lett.* **2006**, *89*, 111120.
(55) McGehee, M. D.; Gupta, R.; Veenstra, S.; Miller, E. K.; Diaz-Garcia, M. A.; Heeger, A. J. Amplified spontaneous emission from photopumped films of a conjugated polymer. *Phys. Rev. B: Condens. Matter Mater. Phys.* **1998**, *58*, 7035−7039.
(56) Rempel, J. Y.; Trout, B. L.; Bawendi, M. G.; Jensen, K. F. Density Functional Theory Study of Ligand Binding on CdSe (0001), (000$\bar{1}$), and (11$\bar{2}$0) Single Crystal Relaxed and Reconstructed Surfaces: Implications for Nanocrystalline Growth. *J. Phys. Chem. B* **2006**, *110*, 18007−18016.
(57) Gómez, D. E.; van Embden, J.; Jasieniak, J.; Smith, T. A.; Mulvaney, P. Blinking and Surface Chemistry of Single CdSe Nanocrystals. *Small* **2006**, *2*, 204−208.
(58) Richter, T. V.; Stelzl, F.; Schulz-Gericke, J.; Kerscher, B.; Wurfel, U.; Niggemann, M.; Ludwigs, S. Room temperature vacuum-induced ligand removal and patterning of ZnO nanoparticles: from semi-conducting films towards printed electronics. *J. Mater. Chem.* **2010**, *20*, 874−879.
(59) Geryak, R.; Tsukruk, V. V. Reconfigurable and Actuating Structures from Soft Materials. *Soft Matter* **2014**, *10*, 1246−1263.
(60) Mamedov, A. A.; Belov, A.; Giersig, M.; Mamedova, N. N.; Kotov, N. A. Nanorainbows: Graded Semiconductor Films from Quantum Dots. *J. Am. Chem. Soc.* **2001**, *123*, 7738−7739.
(61) Shopova, S. I.; Farca, G.; Rosenberger, A. T.; Wickramanayake, W. M. S.; Kotov, N. A. Microsphere whispering-gallery-mode laser using HgTe quantum dots. *Appl. Phys. Lett.* **2004**, *85*, 6101−6103.
(62) Kharlampieva, E.; Kozlovskaya, V.; Zavgorodnya, O.; Lilly, G. D.; Kotov, N. A.; Tsukruk, V. V. pH-responsive photoluminescent LbL hydrogels with confined quantum dots. *Soft Matter* **2010**, *6*, 800−807.
(63) Naik, G. V.; Shalaev, V. M.; Boltasseva, A. Alternative Plasmonic Materials: Beyond Gold and Silver. *Adv. Mater.* **2013**, *25*, 3264−3294.
(64) Ramezani, H.; Kottos, T.; El-Ganainy, R.; Christodoulides, D. N. Unidirectional nonlinear *PT*-symmetric optical structures. *Phys. Rev. A: At., Mol., Opt. Phys.* **2010**, *82*, 043803.
(65) Regensburger, A.; Bersch, C.; Miri, M.-A.; Onishchukov, G.; Christodoulides, D. N.; Peschel, U. Parity−time synthetic photonic lattices. *Nature* **2012**, *488*, 167−171.
(66) Bae, W. K.; Nam, M. K.; Char, K.; Lee, S. Gram-Scale One-Pot Synthesis of Highly Luminescent Blue Emitting $Cd_{1-x}Zn_xS$/ZnS Nanocrystals. *Chem. Mater.* **2008**, *20*, 5307−5313.
(67) Kharlampieva, E.; Slocik, J. M.; Singamaneni, S.; Poulsen, N.; Kröger, N.; Naik, R. R.; Tsukruk, V. V. pH-responsive photo-luminescent LbL hydrogels with confined quantum dots. *Adv. Funct. Mater.* **2009**, *19*, 2303−2311.
(68) Cooper, J. K.; Franco, A. M.; Gul, S.; Corrado, C.; Zhang, J. Z. Characterization of Primary Amine Capped CdSe, ZnSe, and ZnS Quantum Dots by FT-IR: Determination of Surface Bonding Interaction and Identification of Selective Desorption. *Langmuir* **2011**, *27*, 8486−8493.
(69) Würth, C.; Grabolle, M.; Pauli, J.; Spieles, M.; Resch-Genger, U. Relative and absolute determination of fluorescence quantum yields of transparent samples. *Nat. Protoc.* **2013**, *8*, 1535−1550.

DOI: 10.1021/acsphotonics.5b00743
ACS Photonics 2016, 3, 647−658

(70) McConney, M. E.; Singamaneni, S.; Tsukruk, V. V. Probing Soft Matter with the Atomic Force Microscopies: Imaging and Force Spectroscopy. *Polym. Rev.* **2010**, *50*, 235−286.

DOI: 10.1021/acsphotonics.5b00743
ACS Photonics 2016, 3, 647−658